3
Texture and Texture Analysis in Engineering Materials

Heinz-Günter Brokmeier and Sang-Bong Yi

3.1
Introduction

The crystallographic texture describes the orientation distribution of the crystallites in a polycrystalline sample and is one of the basic parameters to characterize polycrystalline materials. General introductions in texture analysis can be found in the textbooks by Wassermann and Grewen [1], Bunge [2], Kocks et al. [3], and Bunge and Esling [4]. Texture analysis is a statistical method so that a sufficient number of crystallites given by their crystal coordinate system K_A (Figure 3.1) are needed. Firstly, the orientation distribution has to be related to a sample coordinate system K_B using the orientation g of all grains. The sample coordinate system can be given by the deformation mode or by the shape of the sample. In Figure 3.1, the sample coordinate system is given for a rolling process (RD – rolling direction, TD – transverse direction, and ND – normal direction). Similar to the rolling geometry, geologists define a sample coordinate system by the foliation (equivalent to the rolling plane) and the lineation (equivalent to RD). The resulting orientation distribution function $f(g)$ gives the volume fraction dV of grains in an orientation increment dg. For a detailed description of different ways to define the rotation g by Euler angles, by $(h\ k\ l)[u\ v\ w]$-values, or by the orientation matrix, see Bunge [2].

Secondly, the orientation distribution may depend on the location of the volume element inside a compact sample, so that a texture gradient is observed. Typical examples are more or less all semifinished products. Consequently, the crystal orientation has to be analyzed not only related to the sample coordinate system but also to the position x, y, z in the sample, which is called orientation stereology [5].

Thirdly, the measured crystallographic texture documents the present state of the material. Any thermomechanical treatment or aging can change the texture, so that during the treatment the texture changes with time as a function of process parameters. For a detailed understanding of such processes, it is of great interest to follow the texture changes during the process. Therefore, recently

Neutrons and Synchrotron Radiation in Engineering Materials Science: From Fundamentals to Material and Component Characterization
Edited by Walter Reimers, Anke Rita Pyzalla, Andreas Schreyer, and Helmut Clemens

ISBN: 978-3-527-31533-8

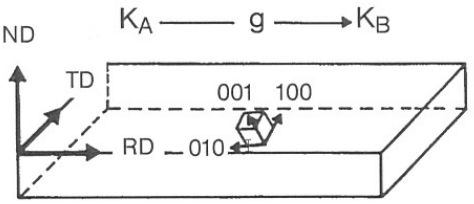

Figure 3.1 Definition of the orientation g of an individual grain. K_A is the coordinate system of a crystallite, K_B is the sample coordinate system with the labeled directions RD (rolling direction), TD (transverse direction), and ND (normal direction).

developed methods for *in situ* experiments [6–8] need fast scanning possibilities adapted to the reaction speed of, e.g., recrystallization or loading.

Fourthly, also the orientation stereology is a function of the external conditions acting on the material that can change with time, see for instance, nucleation processes. However, automatic scanning of crystallite orientations over a sufficient number of individual grains requires a certain amount of time and, thus, the use of this method for the investigation of time-dependent processes where, e.g., the temperature changes with time, is limited. In Table 3.1, a summary of multidimensional texture analyses with up to nine dimensions is given.

Due to the crystallographic structure, material properties of single crystals are anisotropic, so that the crystallographic texture also describes the anisotropy of the material properties of a polycrystal. Consequently, the anisotropy in the material properties of a polycrystalline-textured material (like, e.g., Young's modulus, electric conductivity, thermal expansion, plastic anisotropy, or magnetic behavior) is between single crystal anisotropy and isotropic behavior of a texture-free powder (Figure 3.2). Thus, the knowledge of texture is essential for under-

Table 3.1 Summary of different texture definitions.

Dimension	Experiment
Two-dimensional texture	Pole figure, inverse pole figure
Three-dimensional texture	Orientation distribution function (ODF)
Six-dimensional texture	Orientation stereology Crystal orientation as a function of x, y, z
Six-dimensional texture	Orientation distribution function (ODF) as a function of temperature, time, and mechanical loading
Nine-dimensional texture	Orientation stereology, as a function of temperature, time, and pressure

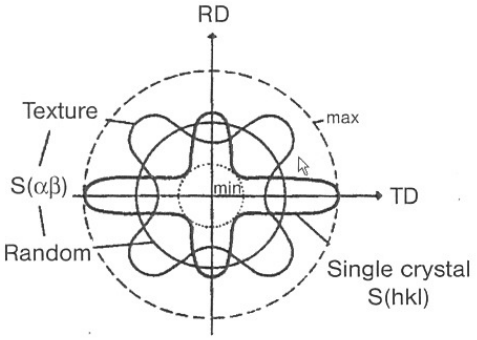

Figure 3.2 Single crystal and polycrystal anisotropy.

standing the properties of technical polycrystalline materials. Here, one has to distinguish on one hand the texture type, which is the qualitative information, from the texture sharpness on the other hand, which gives also quantitative information. A well-known example of the influence of crystallographic texture on the deformation behavior is shown in Figure 3.3, where deep drawing produces an uneven rim of an Al can show the appearance of four ears.

In the last decades, there have been significant advances in texture measuring techniques. These originate not only from technical progresses in instrumentation, computer, and detector technologies, but also from the increasing request for understanding the mechanism of texture evolution which appears unavoidably in thermomechanical processing of almost all polycrystalline materials, such as metals, ceramics, or rocks. The need for efficient use of materials in industrial processes increased the interest in quantitative texture analysis as an effective tool for understanding materials behavior. In this sense, the directional anisotropy of physical and mechanical properties of textured materials is the driving force for advances in quantitative texture analysis. These advances go hand in hand with progress in numerical methods and software development based, e.g., on the series expansion [2, 9] and the WIMV [10, 11] algorithms for the calculation of orientation distribution functions from measured pole figures. Current topics in

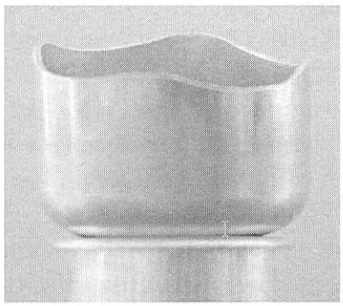

Figure 3.3 Al deep drawing cup showing the earing effect.

Table 3.2 Penetration power of different radiations as half value thickness $I/I_0 = 50\%$.

Metal	X-ray Cu Kα 1.54 Å	s-ray 0.124 Å–100 keV	S-ray 0.062 Å–200 keV	n-ray 1.00 Å
Mg	0.0140 cm	3.40 cm	4.20 cm	6.10 cm
Al	0.0053 cm	1.50 cm	2.70 cm	7.67 cm
Cu	0.0015 cm	0.20 cm	0.50 cm	0.85 cm
Ti	0.0011 cm	0.60 cm	1.30 cm	1.61 cm
Pb	0.0003 cm	0.03 cm	0.04 cm	2.10 cm

texture analysis are, e.g., prediction of anisotropic behavior, optimization of textures for industrial applications, and new aspects in texture research like modeling and simulation of polycrystalline plasticity.

In this chapter, texture-measuring techniques that nowadays are widely used will be introduced and compared to each other. By comparing each method, the necessities for the use of large-scale facilities in texture analysis and the importance of selecting the adequate equipment for user demands will be emphasized. An important issue is the penetration depth because it largely determines the experimental technique to be used for a specific problem. In Table 3.2, penetration depths of different types of radiation are collected. Finally, characteristics of diffraction methods will be presented with selected examples.

3.2 Pole Figures

Pole figures are used for the graphical representation of textures. A pole figure is a projection of directions on a plane. Often the stereographic projection is used, which is shown in Figure 3.4a. A direction is defined by a line from the center of a sphere (O) to a point on the surface of the sphere (A). The direction can be, e.g., the normal of a set of lattice planes. When the point A is observed from the point P, the point of intersection B marks the stereographic projection of the direction $\overline{OA}$ on a plane. Directions determined in this way can be drawn into a polar grid (Figure 3.4b). When the intensity distribution gained from the measurement of a lattice reflection with indices $h\ k\ l$ where the sample is rotated around two axes (angles α and β) is drawn into such a polar grid using contour lines, it is called a pole figure. The diffracted intensity is proportional to the fraction of crystallites within the tested volume oriented in the specific direction.

Three angles are required for defining the orientation of a crystallite in relation to the sample axes, where different sets of angles are possible. A common choice is the set of Euler angles φ_1, ϕ, and φ_2 for the consecutive rotations around the

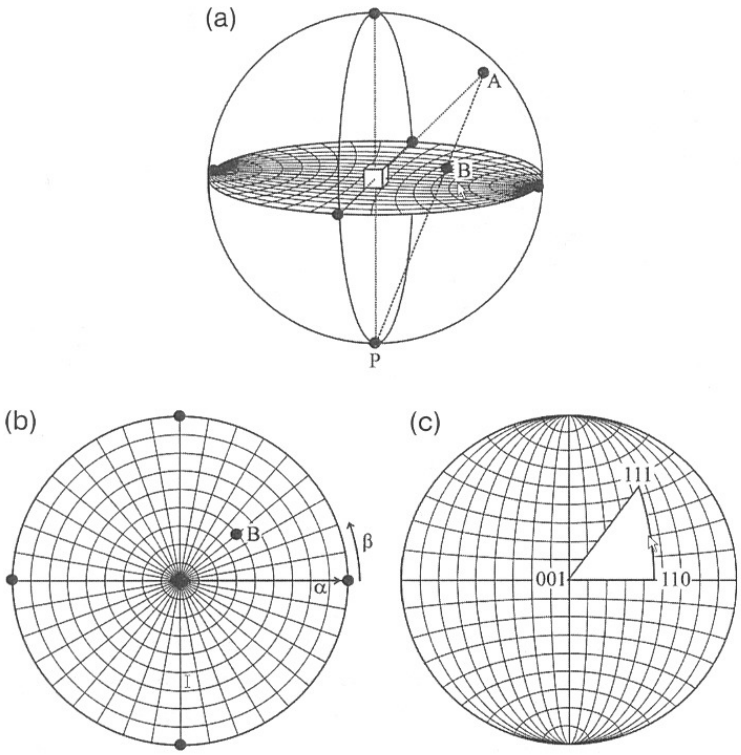

Figure 3.4 (a) Stereographic projection (see the text). (b) Polar grid in which pole figures are drawn. (c) Part of a polar grid used for inverse pole figures in cubic materials.

z-axis, x-axis, and again z-axis [2]. Mathematically, texture can be described by the orientation distribution function (ODF) $f(g)$ with the orientation $g(\varphi_1, \phi, \varphi_2)$. Since the diffracted intensity does not depend on the rotation angle around the scattering vector, two or more pole figures have to be determined for a calculation of the ODF, where the required number of pole figures and suitable choices of $h\ k\ l$ depend on the crystal symmetry and on the sample symmetry. Orientation distribution functions are usually plotted for a set of different values of φ_1 (e.g., every 5°), for each φ_1, the distribution is drawn as a contour plot with the orthogonal axes ϕ, φ_2 [2]. A very practical description of the orientation distribution function, which can be calculated from φ_1, ϕ, φ_2, is the lattice plane $(h\ k\ l)$ parallel to the rolling direction and the lattice direction $[u\ v\ w]$ parallel to the rolling direction.

A representation of the crystal orientation with respect to a sample orientation, e.g., a wire axis or rolling or transverse direction in a rolled sheet, is called inverse pole figure. Only a part of the polar grid is required for such a representation, depending on the crystal symmetry of the material (Figure 3.4c). It has to be noticed that any sample orientation has its own inverse pole figure.

3.3
Texture Measurements on Laboratory Scale

3.3.1
X-ray Diffraction

As a standard laboratory method, X-ray diffraction is the most commonly used for texture measurements. The essential set-up of an X-ray texture diffractometer consists of an X-ray tube, a detector, and a four-circle goniometer that is called Eulerian cradle. Two methods of pole figure measurement are generally used, reflection and transmission geometry (Figure 3.5). The sample is rotated around two axes, tilting (χ in reflection and ω in transmission) and rotation (ϕ in reflection and χ in transmission) at fixed detector position (2θ) for a certain crystallographic plane. Because X-rays are strongly absorbed by matter, the transmission geometry is applicable to thin foils or materials with low absorption. Figure 3.6 represents the pole figure grid of 5×5 in tilting and rotation, and the pole figure coverage at one sample position by using different type of detectors. More than one pole figure can be measured simultaneously by using a one-dimensional position sensitive detector (line detector) covering more than one reflection. In addition, several measuring points in each pole figure can be covered simultaneously by using a two-dimensional position sensitive detector (area detector).

Because of the low penetration power and small beam size in laboratory X-ray diffraction, when compared to those for neutrons (Table 3.2), poor grain statistics are achieved in coarse-grained materials. To increase the grain statistics, sample oscillation over some millimeters or more is used during the measurement under the assumption of homogeneous texture in the oscillated area. Another way of raising the statistics is to add the pole figures measured at more than one position (or sample). Due to the strong defocusing effect and the diffraction geometry, complete pole figures cannot be measured by laboratory X-ray diffraction. In reflection geometry, the pole figure measurement is carried out in general up to $\chi = 70^\circ$ or at most $\chi = 85^\circ$. On the contrary, the peripheral part of the pole figure is covered in transmission geometry. In transmission, pole figures are measured up to $\omega = 55^\circ$ or at most $\omega = 60^\circ$. Diverse methods are used to obtain complete

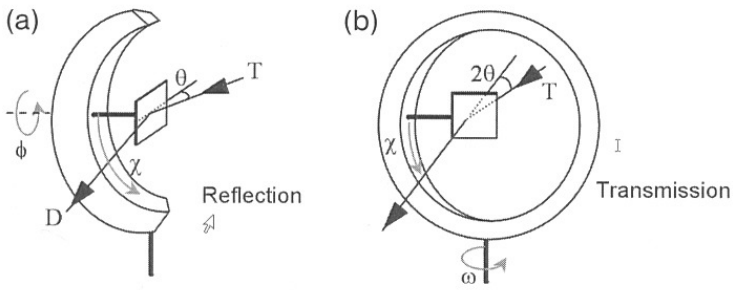

Figure 3.5 Diffraction geometry in pole figure measurements: (a) in reflection and (b) in transmission.

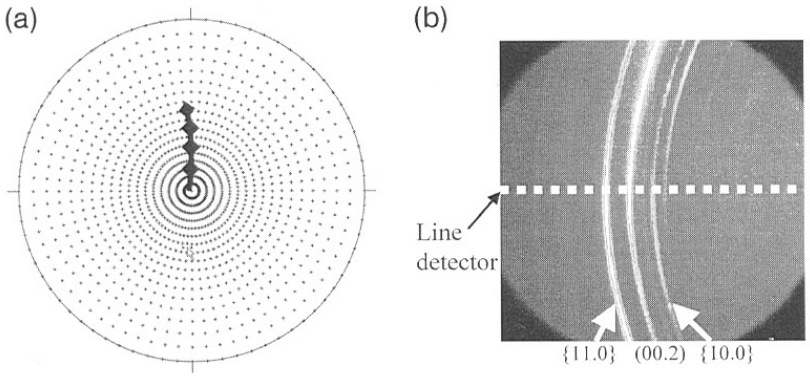

Figure 3.6 (a) Pole figure measuring grid with 5 × 5 in tilting and rotation. Each grid point is measured individually by a point or line detector. (b) Diffraction image of extruded Mg on an area detector. The pole figure coverage by one diffraction line on this image, e.g., (0 0 2), is marked in (a) with a black line.

pole figures, e.g., recalculation of the pole figure from the orientation distribution function (ODF), combination of transmission with reflection method, or the use of oblique samples [12].

However, the last two methods are seldom used due to difficulties in measurement and sample preparation, while the ODF calculation has become a standard procedure in X-ray texture analysis. It is often found in practical measurements that some diffraction peaks are located very close to each other or totally overlapped, especially in polyphase samples and/or materials with low crystal symmetry. In such cases, the overlapped peaks are hardly to be used for pole figure measurements unless mathematical peak fitting can be employed to separate the peaks. Despite of the above limitations, laboratory X-ray diffraction technique is the most widely used for texture analysis, because of the easiness in machine usage, low cost, and relatively easy sample preparation.

3.3.2 Electron Diffraction

Orientation determination by electron diffraction is accomplished by indexing of the so-called Kikuchi patterns or spot diffraction patterns, using, e.g., selected area diffraction (SAD) or small-angle convergent beam electron diffraction (SCBED). Figure 3.7 illustrates the formation of the Kikuchi line and SCBED spot pattern. The Kikuchi patterns in SEM and TEM are formed in similar way. The only difference is that in SEM the backscatter electrons have an opposite direction to the incident beam, while in TEM transmitted electrons form the Kikuchi pattern. When an electron beam is directed onto a crystalline sample, electrons are scattered from lattice planes according to Bragg's law. These inelastically scattered electrons emerge along diffraction cones having an opening

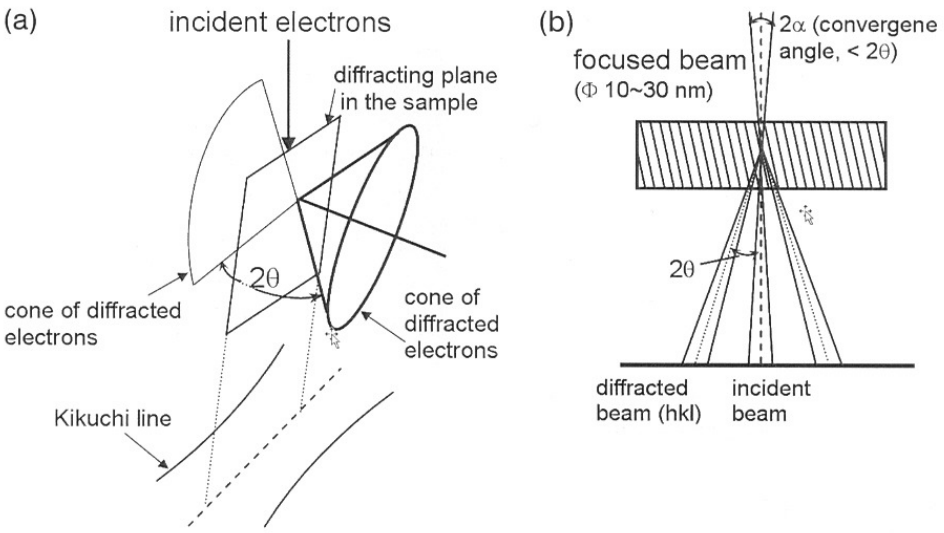

Figure 3.7 (a) Kikuchi line formation in TEM. (b) Spot pattern in TEM–SCBED, Kossel–Möllenstedt pattern in the case of $2\alpha < 2\theta$ [15].

angle of $180° - 2\theta$. When the cones of diffracted electrons intersect a detecting screen, they form Kikuchi lines on the screen. The usage of SCBED in TEM results in significant improvement in spatial resolution of below 10 nm, while SAD delivers average information from about 0.5 μm [13]. Once the electron beam is focused to a smaller convergence angle (2α) than the diffraction angle (2θ), the nonoverlapped spot pattern by elastic diffraction of electrons is observed on the TEM screen, called Kossel–Möllenstedt pattern. For a detailed description of electron diffraction, see Refs. [14, 15]. With the aid of the current developments in electron microscopy, computer techniques, and automated pattern indexing, e.g., Kikuchi pattern indexing based on the Hough transformation [15] or SAD spot pattern indexing by template matching [16], electron diffraction has become an important tool for microstructure and texture analysis. The real power of electron diffraction in materials analysis lies in the simultaneous determination of both orientation and microstructure with high angular and lateral resolution at defined sample positions. Also, energy dispersive X-ray chemical analysis (EDX) can be carried out simultaneously with orientation mapping. Based on the above possibilities, texture components can be separated with respect to microstructural elements, e.g., chemical composition, grain size, phase, position, etc. Another important feature of electron diffraction is the possibility of direct texture measurement, i.e., the three-dimensional orientation at the measuring point is determined from indexing the diffraction patterns. Therefore, the results from electron diffraction can be presented directly in the orientation space without additional mathematical calculations, which are necessary in X-ray and neutron measurements. Based on this feature, possible errors occurring during mathematical treatments can be avoided in electron diffraction. However, long-time and large-scaled mapping is necessary to reach satisfactory statistics for deter-

mining the global texture, which is hardly to get in TEM. The diffraction quality is very sensitive to sample conditions, e.g., sample surface flatness, grain size, dislocation density, electric conductivity, etc. In electron backscatter diffraction (EBSD) in SEM, the electrons penetrate only some tens of nanometers such that the pattern quality is even more sensitive than in TEM. It is generally recommended to use high-beam currents for getting a high signal-to-noise ratio in SEM–EBSD and also to apply electropolishing for preventing sample damages during preparation.

3.4
Texture Measurements at Large-Scale Facilities

3.4.1
Neutron Diffraction

The advantages of neutron diffraction lie in the combination of high penetration depth (at some centimeter level) for almost all materials (Table 3.2) and the relatively large beam cross-sections. Thus, the typical sample geometry is completely different from laboratory X-ray and EBSD samples (Figure 3.8). Moreover, complete pole figures are obtained without special sample preparation, and measured pole figures can be used for ODF calculation after background intensity corrections. These characteristics make neutron diffraction a powerful tool for

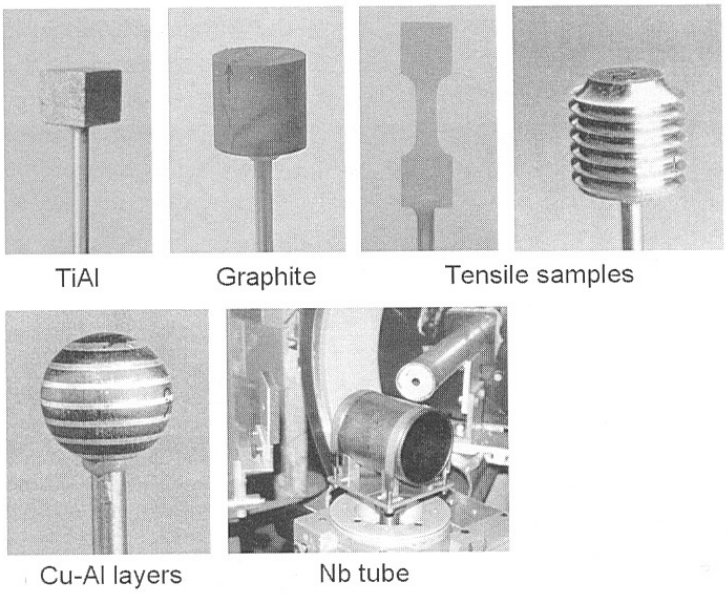

Figure 3.8 Various sample geometries for neutron texture measurements. The sample volume varies from some mm^3 to cm^3, depending on the sample material.

texture analysis, e.g., in geological materials as well as in metallic samples having a complex shape or a large volume. Due to the low absorption for neutrons, satisfactory grain statistics are easily obtained for coarse-grained materials. *In situ* pole figure measurements are possible under various sample environments. The basic principle of pole figure measurement with neutrons is analogous with that of laboratory X-ray reflection. However, longer counting times are often necessary because of the low neutron flux from a reactor. Because of long counting times and possible flux variations depending on reactor conditions, the flux-controlled measuring scheme is generally employed, i.e., constant neutron flux at a measuring point, not constant measuring time.

Figure 3.9 shows a typical set-up for pole figure measurements using a monochromatic neutron beam. Since thermal neutrons from a reactor cover a wide range in wavelength, in general 0.5–4 Å, a bunch of single crystals is employed for getting a monochromatic beam. The single crystals are located on a plate having a slight curvature such that there is a focused beam at the sample position.

The different wavelengths are easily selected by changing the monochromator take-off angle. Like for X-ray diffraction, line and area detectors are also applicable in neutron diffraction for recording more than one measuring points simultaneously (Figure 3.6). Another way to cover several reflections simultaneously is use of the time-of-flight (TOF) method with neutrons. The wavelength of a neutron is inverse proportional to its velocity so that a polychromatic neutron beam can be analyzed with regard to the flight time of the neutrons. In TOF measurements, the diffraction angle (θ in Bragg's law) remains constant, hence a lattice spacing (d in Bragg's law) profile is achieved based on the wavelength pattern. A long flight path of neutrons is necessary for high resolution in time-of-flight analysis. Since the whole diffraction profile, according to the wavelength range, is measured at once, for example, 0.5–4 Å of wavelength range corresponds to the d-spacing of 0.35–2.83 Å at fixed $\theta = 45°$, the TOF technique is well suited for low crystal symmetric as well as for multiphase samples. The wide range of the measured diffraction profile can be directly utilized for the whole diffraction profile analysis, e.g., Rietveld refinement-based texture analysis and structure analysis

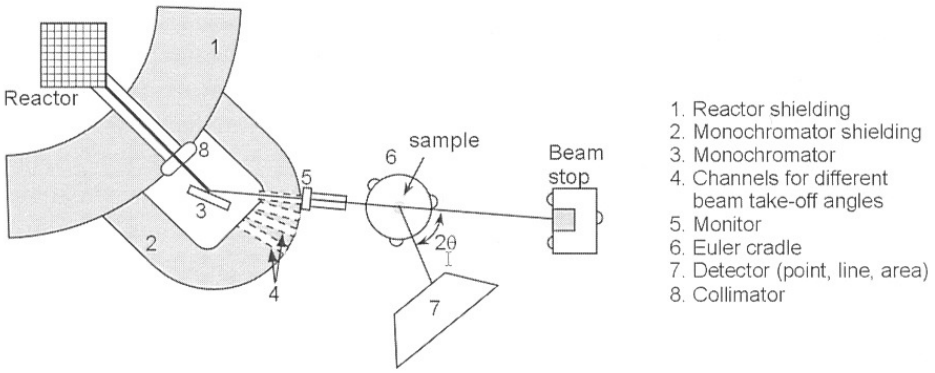

Figure 3.9 Neutron texture diffractometer TEX-2, GKSS Research Centre, Germany.

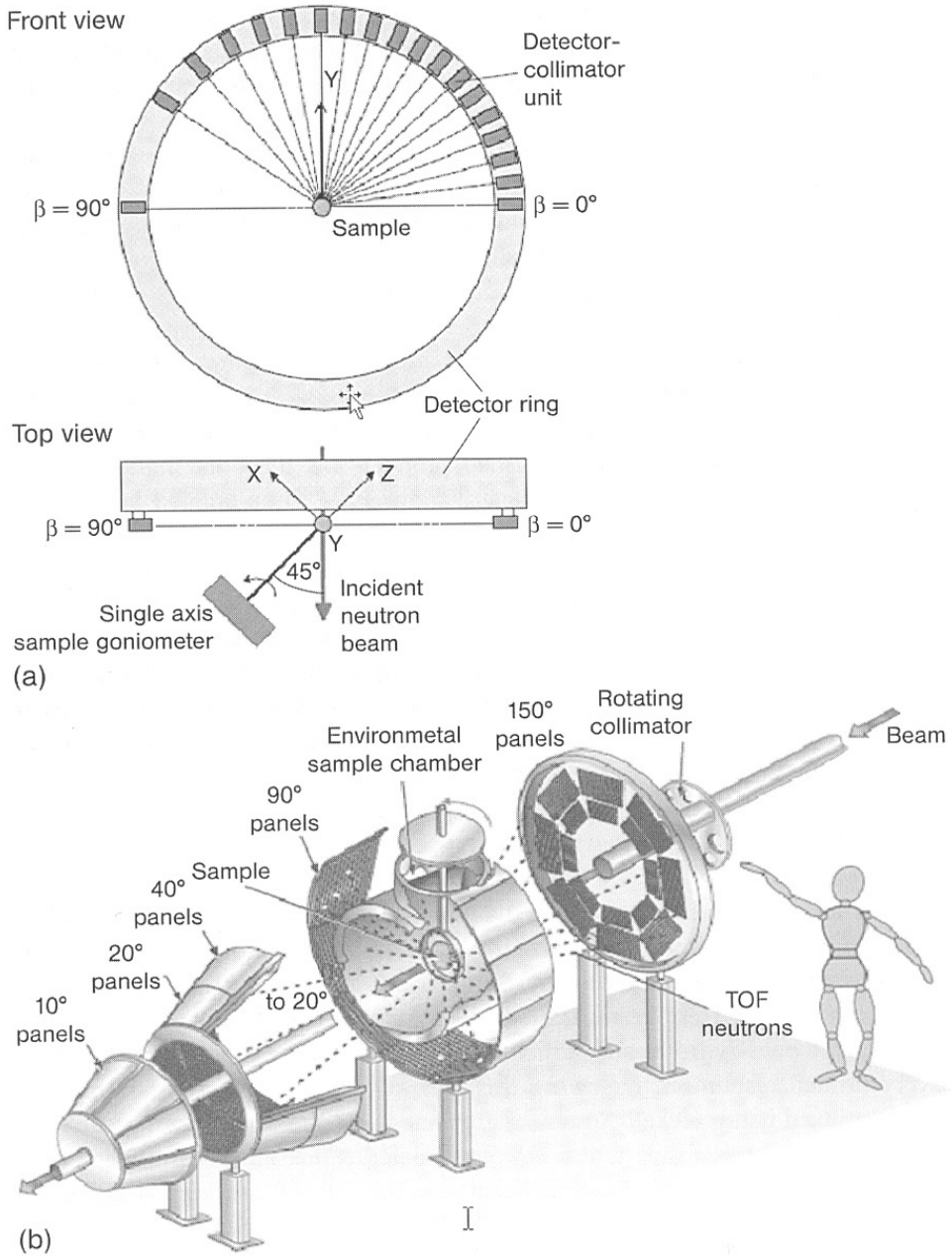

Figure 3.10 Examples of TOF diffractometers with many detectors. (a) SKAT in Dubna, Russia [17]. (b) HIPPO in Los Alamos, USA [18].

[10, 16]. An example of texture analysis using Rietveld refinement will be given in Section 3.4.1.1. With the installation of many detectors at a TOF beam line, complete pole figures can be measured by rotation around one sample axis only. This capability also allows *in situ* texture analysis. Figure 3.10 shows two different

TOF diffractometers equipped with many detectors, the SKAT diffractometer with 19 detectors at the IBR2 Dubna Research Centre in Russia [18] and the HIPPO diffractometer with the total of 1360 detectors at the Los Alamos Laboratory in the USA [19].

Neutrons are a powerful probe for texture analysis not only in the case of coarse-grained material or for measurement of complete pole figures or weak textures, but also for nondestructive texture analysis in semifinished products, which shall be demonstrated in the following example.

3.4.1.1 Texture of Semifinished Products

For texture investigations of semifinished products, there are special requirements for the experimental facilities. On the one hand, in most cases texture varies over the sample volume, which requires determination of the texture at different locations within a semifinished product. On the other hand, often a whole set of different material characterizations have to be applied to identical samples (e.g., qualitative and quantitative phase analysis, stress determination, and texture investigations). In the ideal case, texture analyses are performed nondestructively so that other experimental tests (e.g., a tensile test) can be applied afterward to exactly the same samples. However, a large number of texture investigations are still done destructively by sectioning a large sample due to the limited availability of nondestructive methods. In all these cases, the standard techniques described in this chapter are in use. Nondestructive measurements are nonstandard techniques, so that only a few investigations have been carried out up to now. In all the cases, for avoiding artifacts due to sample preparation, particularly on the sample surface, a beam with a high penetration power is needed (Table 3.2).

In the case of nondestructive investigations, the sample shape influences the texture measurement due to a changing illuminated volume and changing absorption during sample rotation and tilting. In some cases, one has to work with incomplete pole figures. In such an extreme case, even just a few characteristic points in the pole figure can be sufficient to calculate an ODF, however, only with a very limited resolution. Following this idea, a very practical and fast method can be utilized using 60 keV X-rays for characterizing the deep drawing behavior of 2 mm thick steel strips and a few millimeters thick aluminum strips during sheet production [20]. Such fast and simple methods are very effective for quality insurance purposes in industrial production lines. Nevertheless, to get more precise quantitative texture information, a set of complete pole figures is necessary.

For relatively simple sample geometries like tensile test samples or long cylindrical samples most corrections (constant volume, constant absorption) have only a minor influence on the result or can be neglected [21]. But more complicated is the nondestructive measurement of textures in semifinished products like tubes using the reflection method and an absorption correction [22], which shall be shown with the following examples. A Nb-tube of 140 mm length, 84 mm diameter, and 3 mm wall thickness shown in Figure 3.11 was investi-

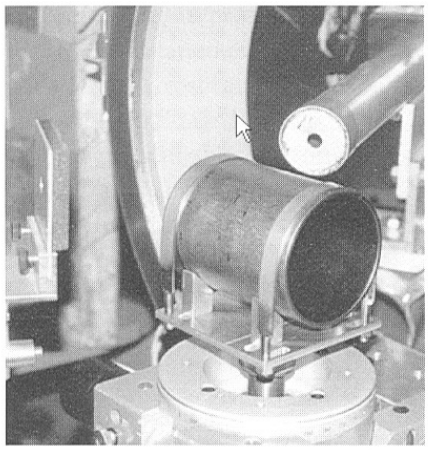

Figure 3.11 Photograph of a Nb tube mounted in the texture diffractometer TEX-2 at GKSS.

gated with respect to texture anisotropy around the perimeter. Seamless cavities for the manufacturing of accelerator units for a linear collider are produced from such tubes by hydroforming. A texture variation around the perimeter of the tube can lead to uneven cavity formation during the hydroforming step and to a rough inner surface of the tube making such cavities rejects. Local textures averaged over the wall thickness could be obtained from a whole tube with neutron diffraction. This was possible by using 4 mm wide slits on both sides, incoming and outgoing beam. It could be shown that this texture variation was on the one hand due to the texture of the ingot the tube was produced from, and on the other hand to the low deformation degree during tube manufacturing [22].

Seamless cavities made of a Cu–Nb composite are other candidates for the manufacturing of accelerator units for a linear collider. In this case, a composite Cu–Nb tube is the preproduct for hydroforming, which is produced by coextrusion of a Cu and a Nb-tube, or by explosive bonding of a Cu and a Nb-tube [23]. In both the cases, a homogeneous texture around the perimeter and sufficient material flow is required. Besides the type of initial materials, such as the type of the used Cu alloy and the purity of Nb, the production process itself is of great interest. Figure 3.12a shows a Cu–Nb ring, 140 mm in diameter and 15 mm wide, cut from a coextruded tube with additional flow forming to get a tube wall of 4 mm thickness (1 mm Nb and 3 mm Cu). Three pole figures of each phase allow the ODF calculation of the Nb and the Cu part of the composed tube (Figure 3.12b). The ODF section $\varphi_1 = 0^\circ$ with Φ from 0° to 90° and φ_2 from 0° to 90° shows the typical BCC-texture with a strong α-fiber at φ_2 45° and Φ from 0° to 90°. The anisotropy of the Nb texture around the perimeter is shown for three points in Figure 3.12c with different α-fibers for three positions [23]. These investigations were carried out at the neutron texture diffractometer TEX-2 (FRG-1, Geesthacht).

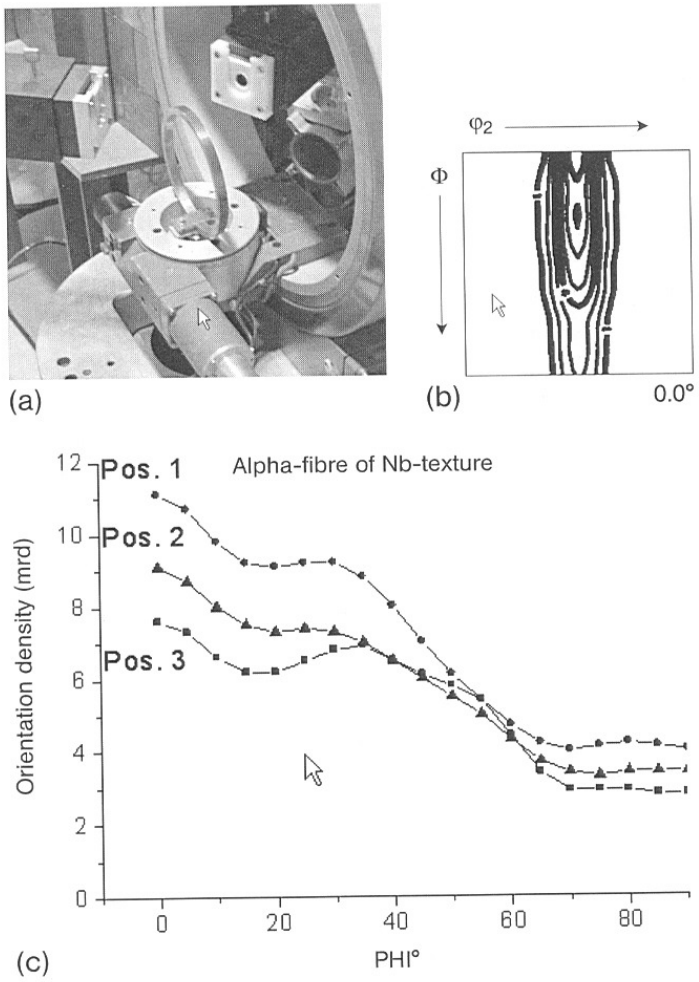

Figure 3.12 Analysis of texture variation in a Cu–Nb ring. (a) Cu–Nb ring mounted in a Eulerian cradle. (b) ODF section for $\varphi_1 = 0°$ of the Nb texture. (c) α-Fibers of the Nb texture for three positions along the perimeter of the tube.

3.4.2 Texture Analysis Using Synchrotron X-rays

Synchrotron X-rays are attractive for texture analysis because of high spatial resolution combined with excellent brilliance and high penetration depth for many materials in the same order as for thermal neutrons. The high spatial resolution results from the highly intense X-ray beam with possible sizes down to a few micrometers. In addition, the divergence of synchrotron X-rays is extremely small so that high orientation resolutions can also be achieved (<0.01). On the basis of the high photon flux, a few percent sample transmission is already enough for a satisfactory intensity at the detector. For this reason, texture investigations of heavy elements in relatively large volumes are possible in transmission geometry.

By employing an area detector in transmission, full Debye–Scherrer rings are recorded simultaneously such that significant reduction of the measuring time and high angular resolution are obtained. In fact, the texture measurements utilizing synchrotron X-rays began with the advent of area detectors in the mid-1990s. The combination of synchrotron X-rays with area detectors has opened new fields in texture analysis. Texture analysis at localized volumes with sizes from micrometers to centimeters is now possible in a nondestructive way. Though neutron diffraction allows nondestructive texture analysis, its spatial resolution is limited to the order of millimeters. Moreover, synchrotron X-rays offer the possibility for *in situ* measurements under various sample environments, due to the fast measuring time together with high penetration power and small wavelength. As with the neutron TOF technique, sample revolution along one axis is enough to cover full pole figures, which offers more freedom for sample environment devices.

The principle of pole figure measurement using synchrotron X-rays is similar to that of laboratory X-ray measurement that was introduced already in the beginning of the 20th century using X-ray films as the only available area detector at that time. The main difference is the wavelength, which has a strong influence on the scanning routine (Figure 3.13). Depending on the research interests and machine availabilities, various measuring methods have been developed by many working groups. For the detailed description of other methods, see the following references: stationary and moving detector modes [24, 25], employing a conical slit system using monochromatic beam [26], and energy dispersive method using white beam. In this chapter, the texture measurement using monochromatic beams and area detectors will be introduced, so-called stationary detector mode, as a basic measuring technique available in almost all synchrotron X-ray beam lines without employing special slit systems. Figure 3.13 illustrates the basic beam line set-up for texture measurement at the synchrotron beam line BW5 at Hasylab in Hamburg, Germany. The primary white beam from the wiggler enters the experimental station; the desired wavelength is selected using a mono-

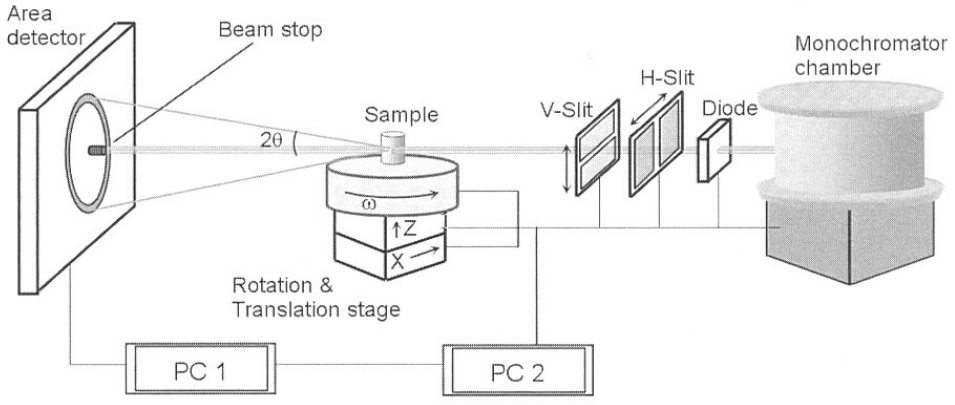

Figure 3.13 Set-up for texture measurements at beam line BW5 at Hasylab, Germany. PC 1 is responsible for reading data from the area detector; PC 2 controls all motors.

chromator located in a vacuum chamber. The beam size is controlled by motorized horizontal and vertical slits. Because a synchrotron beam decays gradually with time and, thus, periodical reinjection of accelerated particles into the storage ring is necessary, the incident beam intensity is monitored at a gas-counter (diode) for the correction of measured intensity (detector). The sample is positioned on a ω-rotation table mounted on a XZ-stage which allows sample translations in sample height (Z) and in the perpendicular direction to the incident beam (X). For a complete texture measurement, the sample is rotated around the ω-axis with a fixed step size. At each ω-position, the sample is irradiated and the occurring Debye–Scherrer rings are collected at the area detector. Since the intensity along the Debye–Scherrer rings is proportional to the pole density on the orientation sphere, the textured sample shows an intensity variation with the angle γ along the ring (Figure 3.14). A Debye–Scherrer ring recorded at a certain sample rotation ω covers a circle in the corresponding $\{h\ k\ l\}$ pole figure and the full pole figure coverage is completed by the ω-rotation. As shown in Figure 3.14, there is a blind area in the pole figure, which originates from the diffraction geometry. Due to the low wavelength, however, this unmeasurable area, which corresponds to the diffraction angle θ, appears only in a small area. In case of using an energy of 100 keV (wavelength of 0.12 Å) the diffraction rings of most interest locate at θ ranges less than 3°.

The task of commonly available programs is the ODF calculation (series expansion and WIMV method), more correctly, the pole figure inversion and normalization, meaning that measured pole figure presented in the $\{\omega, \gamma\}$ grid has to be interpolated into a regular $\{\alpha, \beta\}$ grid. In the following sections, some selected examples of texture analysis using synchrotron X-rays are given.

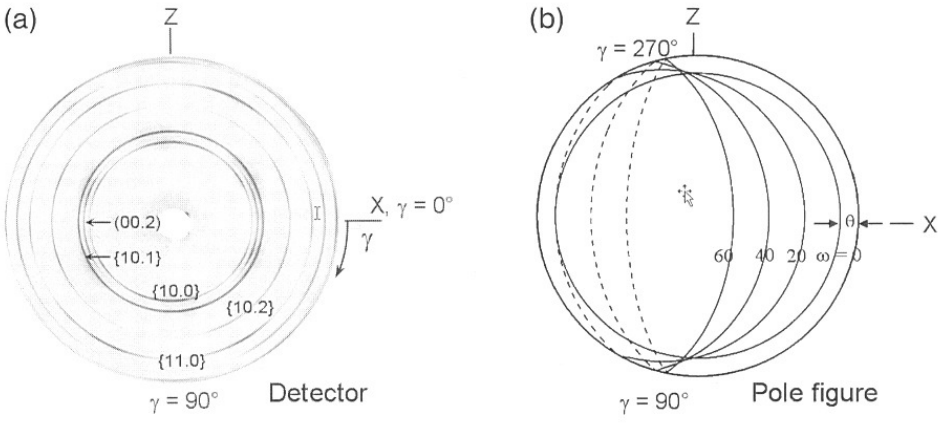

Figure 3.14 (a) Diffraction image from strongly textured Mg on an area detector (transmission method). (b) Pole figure coverage by Debye–Scherrer rings obtained at different ω-positions. Solid lines in the pole figure are corresponding to Debye–Scherrer rings within the range from $\gamma = 90°$ to 270°. For emphasizing the blind area effect, $\theta = 10°$ and equal area projection are applied to this pole figure.

3.4.2.1 Local Texture Measurement in an Extruded Mg Rod

Texture heterogeneity in a round extruded Mg rod, which shows a different texture in core and mantel, was examined by a synchrotron beam having a cross-section of 1 mm × 1 mm [27]. The rod with a diameter of 14 mm was produced by extrusion at 300 °C of precompacted Mg powder (∅74 mm). The sample for the texture measurement with a size of 3 mm × 5 mm × 14 mm was cut with the long edge along a rod diameter (Figure 3.15a). A stronger ⟨1 0 0⟩ fiber texture component parallel to the extrusion direction is observed in the mantel (sample Mg1–0) than in core (sample Mg1–4) of the extruded rod (Figure 3.15b). Looking on the (0 0 2) pole figure the texture variation can be seen as a shift of the (0 0 2) pole. Due to the high brilliance of the synchrotron X-ray, which corresponds to a small pole figure window, the detection of the orientation pole shift in a very small range is also possible. As shown in Figure 3.15c, this pole shift goes from 90° (Mg1–0) to 85° (Mg 1–4). Because of the high texture symmetry, the results are represented by intensity variation along the equator on the (0 0 2) pole figure, so-called linear pole figure.

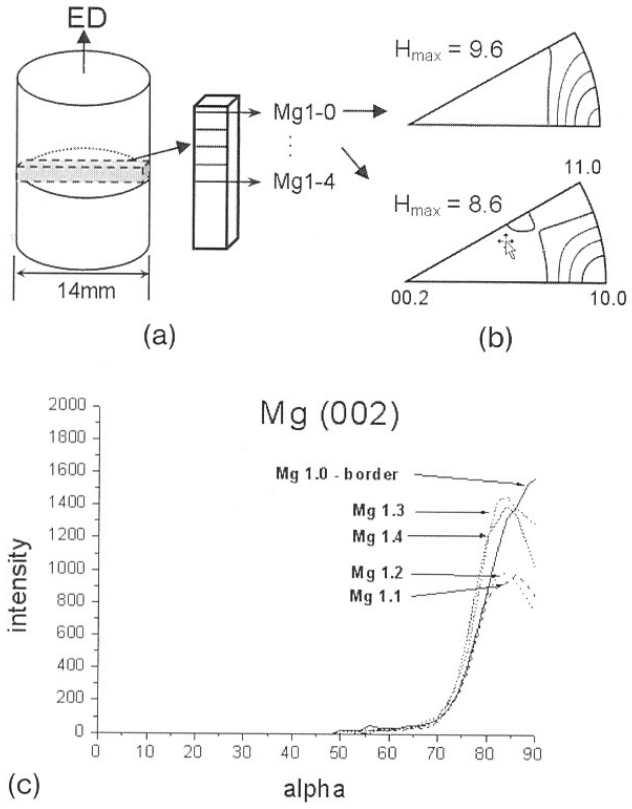

Figure 3.15 (a) Samples for texture measurements cut from an extruded Mg rod (ED stands for the extrusion direction). (b) Inverse pole figures in ED for mantle and core of the rod. (c) Intensity variation along the equator on the (0 0 2) pole figures.

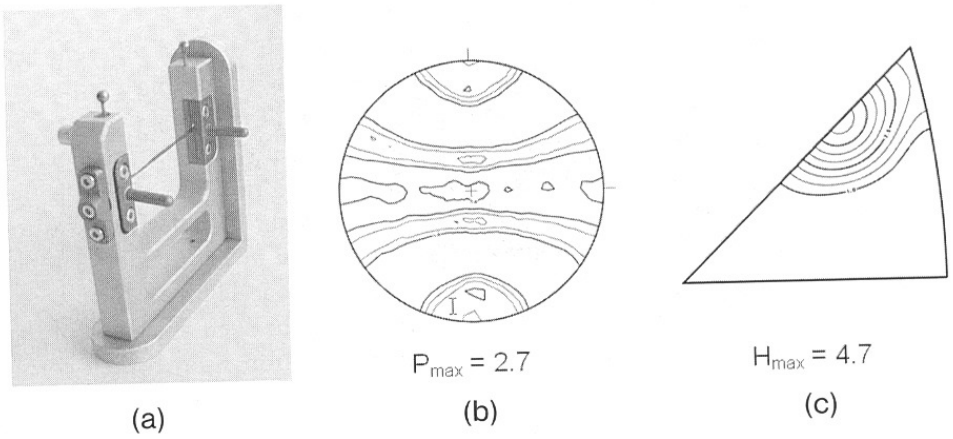

Figure 3.16 (a) Wire sample holder with ten softly stretched Cu wires. (b) The average of six measured (1 1 1) pole figures; the wire direction is in the center of the pole figure. (c) Inverse pole figure for the wire direction.

3.4.2.2 Global Texture in Cu Wire

The determination of the global texture in a Cu wire with a thickness of 0.12 mm is shown in this example [28]. Texture measurement in such a thin wire using other techniques, e.g., electron and neutron diffractions, suffers from grain statistics and low diffraction intensity, respectively. Also, a conventional X-ray measurement needs an intensity correction according to the wire geometry [29]. By employing a specially designed wire holder (Figure 3.16a), which extends slightly the wire bundle, the global texture of the thin wire was successfully obtained. For increasing grain statistics, the measurements were carried out at six different sample positions. Thereafter, the measured pole figures were averaged into one pole figure. The averaged (1 1 1) pole figure (Figure 3.16b) and the inverse pole figure in the wire direction (Figure 3.16c) show a strong $\langle 1\ 1\ 2 \rangle$ fiber texture component parallel to the wire direction.

3.4.2.3 *In situ* Texture Measurement at Elevated Temperatures

Texture transformation, i.e., texture inheritance during phase transformation, was investigated by heating of a steel sample [30]. The texture of plain steel (carbon content: 0.2 mass%) sample, having BCC crystal structure (α-ferrite), was measured at room temperature. Thereafter, the sample was heated until the phase transformation to FCC structure (γ-austenite) was completed. The texture measurement of the γ-austenite was carried out at elevated temperatures. Figure 3.17a shows the vacuum furnace used for the *in situ* texture measurement. The furnace can be installed on the ω-rotation table and causes no additional diffraction peaks. Because of grain growth effects, fast measuring time is basically necessary for this *in situ* measurement. For reducing the measuring time, the ω-rotation was conducted up to 45° with 5° step, which covers only a quarter of

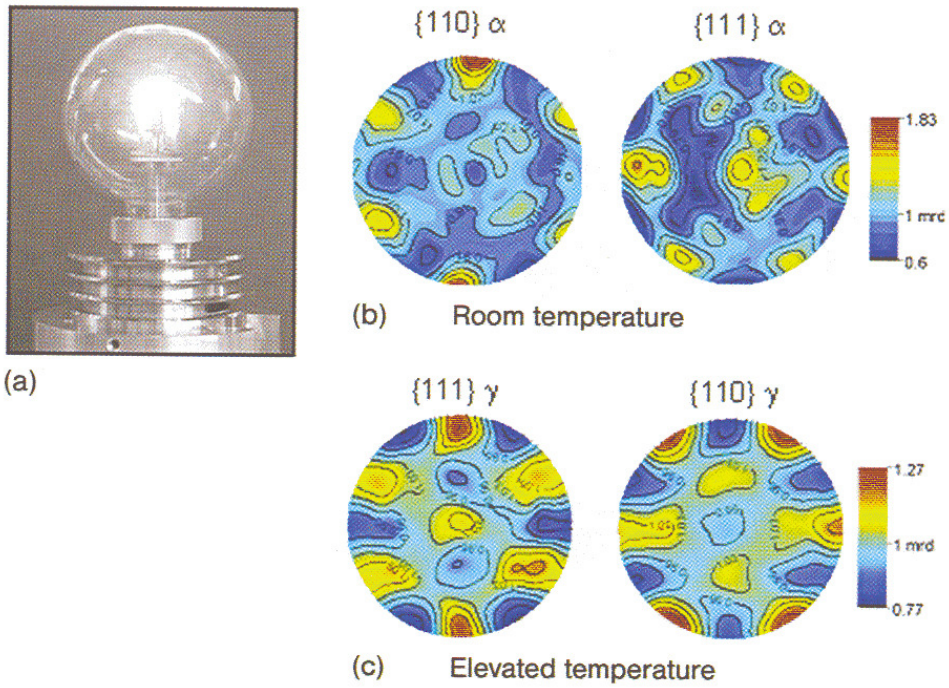

Figure 3.17 (a) Vacuum furnace with glass wall and graphite heating element. Pole figures of (b) α-ferrite and (c) γ-austenite as calculated using the MAUD software.

the pole figure. For extracting the complete pole figures from the restricted data, the Rietveld texture analysis program MAUD [10], which is based on whole diffraction profile analysis, was employed. The calculated pole figures of the α-ferrite and the γ-austenite are shown in Figure 3.17b and c, respectively. The texture results match well to the Kurdjumov–Sachs orientation relationship for BCC ↔ FCC transformation: $(1\ 1\ 1)_{FCC} \| (0\ 1\ 1)_{BCC}$ and $[1\ 0\ 1]_{FCC} \| [1\ 1\ 1]_{BCC}$.

3.4.2.4 *In situ* Texture Measurement Under Loading

In situ measurements guarantee to study the texture evolution without the influence originating from the usage of many different samples. In fact, the mechanical properties and the texture evolution are strongly dependent on the initial texture and microstructure, and this dependency, for example, becomes more pronounced in magnesium alloys having a HCP crystal structure. The texture variation was investigated during uniaxial compression of Mg alloy AZ31 [31]. AZ31 is a Mg-based grade, alloyed with Al and Zn. A universal testing machine (UTM), by which a sample can be loaded up to 20 kN, was installed on the ω-rotation table (Figure 3.18). During the irradiation of the sample for texture measurement, the loading was stopped, but not released, and the sample was rotated together with the UTM around the ω-axis. Figure 3.18b presents the texture vari-

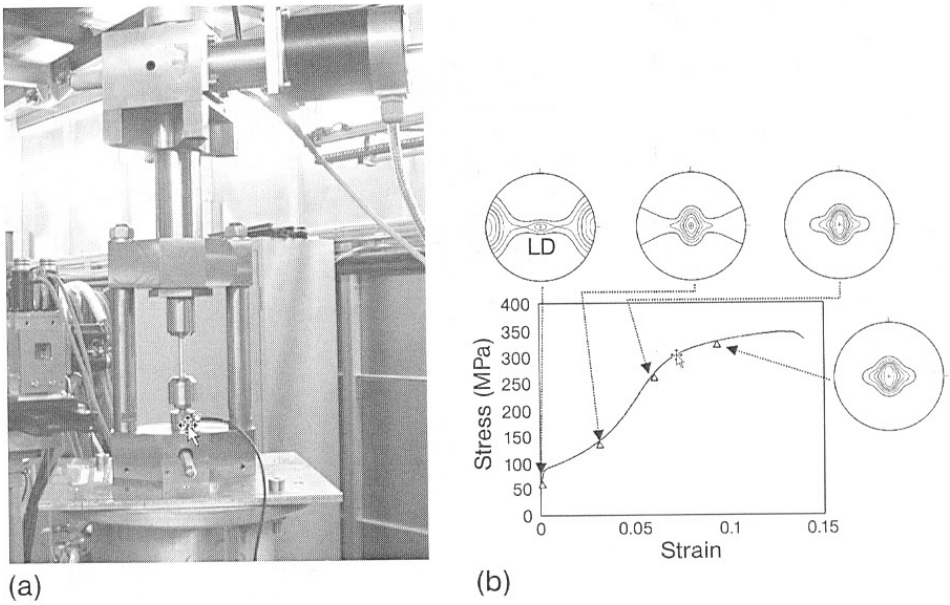

Figure 3.18 (a) UTM installed on the ω-rotation table. (b) Flow curve during compression of AZ31 and (0 0 2) pole figures at different strains. The loading direction (LD) is in the center of the pole figure.

ation in terms of (0 0 2) pole figures and the stress–strain curve during compression. By interpreting the measured texture results together with the results of a numerical simulation of texture development the anisotropic behavior and the activity of the potential deformation modes in a Mg alloy could be analyzed as a function of initial texture and deformation degree.

References

1 G. Wassermann, J. Grewen, *Texturen metallischer Werkstoffe*, 2. Auflage, Springer, Berlin, Göttingen, Heidelberg, 1962.

2 H.J. Bunge, *Texture Analysis in Materials Science*, Cuvillier Verlag, Göttingen, 1993.

3 U.F. Kocks, C.N. Tomé, H.-R. Wenk, *Texture and Anisotropy*, Cambridge University Press, Cambridge, 1998.

4 H.J. Bunge, C. Esling, *Quantitative Texture Analysis*, DGM-Informationsverlag, Oberursel, 1986.

5 H.J. Bunge, R.A. Schwarzer, Orientation stereology–a new branch in texture research, *Adv. Eng. Mater.* 2001, **3**, 25–39.

6 H.-G. Brokmeier, S.B. Yi, N.J. Park, J. Homeyer, In-situ texture analysis using hard X-rays, *Solid State Phen.* 2005, **105**, 55–60.

7 S.C. Vogel, D. Bhattacharyya, G.B. Viswanathan, D.J. Williams, H.L. Fraser, Phase transformation textures in Ti–6Al–4V alloy, *Mater. Sci. Forum* 2005, **495**, 681–686.

8 H.-G. Brokmeier, In-situ texture analysis under applied load rays, in: *Advanced Materials* 2005 eds: M. Farooque, S.A. Rizvi, J.A. Mirza, KRL Rawalpindi, Pakistan 2007, 292–301.

9 M. Dahms, H.J. Bunge, The iterative series-expansion method for quantitative texture anaysis, *J. Appl. Crystallogr.* 1989, **22**, 439–447.

10 S. Matthies, G.W. Vinel, On the reproduction of the orientation distribution function of texturized samples from reduced pole figures using the conception of a conditional ghost correction *Phys. Status Solidi* 1982, **B112**, 111–114.

11 L. Lutterotti, http://www.ing.unitn.it/~maud/.

12 H.J. Bunge, *Experimental Techniques of Texture Analysis*, DGM Informationsgesellschaft Verlag, 1985.

13 S. Zaefferer, Investigation of the correlation between texture and microstructure on a submicrometer scale in the TEM, *Adv. Eng. Mater.* 2003, **5**, 745–752.

14 D.B. Williams, C.B. Carter, *Transmission Electron Microscopy: A Textbook for Materials Science*, Plenum Press, New York, 1996.

15 A.J. Schwartz, M. Kumar, B.L. Adams, *Electron Backscatter Diffraction in Materials Science*, Kluwer Dordrecht, 2000.

16 E.R. Rauch, A. Duft, Orienation maps derived from TEM diffraction patterns collected with an external CCD camera, *Mater. Sci. Forum* 2005, 495–497, 197–202.

17 L. Lutterotti, S. Matthies, H.-R. Wenk, A.J. Schultz, J.W. Richardson, Combined texture and structure analysis of deformed limestone from time-of-flight neutron diffraction spectra, *J. Appl. Phys.* 1997, **81**, 594–600.

18 K. Ullemeyer, P. Spalthoff, J. Heinitz, N.N. Isakov, A.N. Nikitin, K. Weber, The SKAT texture diffractometer at the pulsed reactor IBR-2 at Bubna: experimental layout and first measurements, *Nucl. Instrum. Methods Phys. Res.* 1998, **412**, 80–88.

19 S.C. Vogel, C. Hartig, R.B. Von Dreele, H.-R. Wenk, D.J. Williams, Quantitative texture measurements using neutron time-of-flight diffraction, *Mater. Sci. Forum* 2005, 495–497, 107–112.

20 H.-J. Kopineck, H. Otten, in: *Advances and Application of Quantitative Texture Analysis*, eds. H. J. Bunge, C. Esling, DGM-Informationsgesellschaft, Oberursel, 1991, pp. 153–165.

21 H.-G. Brokmeier, B. Schwebke, J. Homeyer, *Texture investigation on an engine shaft*, *Hasylab Annual Report* 2005, 541–542.

22 H.-G. Brokmeier, W. Singer, H. Kaiser, Neutron diffraction–a tool to optimize processing of niobium tubes, *Appl. Phys.* 2002, **A74**, s1704–s1706.

23 W. Ye, H.-G. Brokmeier, V. Singer, Nondestructive texture analysis of a co-extruded Cu–Nb tube, *Mater. Sci. Forum* 2002, **408**, 185–189.

24 H.R. Wenk, S. Grigull, Synchrotron texture analysis with area detectors, *J. Appl. Crystallogr.* 2003, **36**, 1040–1049.

25 H.J. Bunge, L. Wcislak, H. Klein, U. Garbe, J.R. Schneider, Texture and microstructure analysis with high-energy synchrotron radiation, *Adv. Eng. Mater.* 2002, **4**, 300–305.

26 R.V. Martins, U. Lienert, L. Margulies, A. Pyzalla, Determination of the radial crystallite microstrain distribution within an $AlMg_3$ torsion sample using monochromatic synchrotron radiation, *Mater. Sci. Eng.* 2005, **A402**, 278–287.

27 H.-G. Brokmeier, A. Günther, S.B. Yi, W. Ye, Investigation of local textures in extruded magnesium by synchrotron radiation, *Adv. X-ray Anal.* 2003, **46**, 151–156.

28 H.-G. Brokmeier, B. Weiss, S.B. Yi, W. Ye, K.D. Liss, T. Lippmann, Texture determination of thin Cu-wires by synchrotron radiation, *Mater. Sci. Forum* 2005, 495–497, 131–136.

29 T. Montesin, J.J. Heinzmann, A. Vadon, Absorption corrections for X-ray texture measurement of any shape sample, *Textures Microstruct.* 1991, **14**, 567–572.

30 H.-G. Brokmeier, S.B. Yi, B. Schwebke, J. Homeyer, *In situ* analysis of crystallographic texture using high-energy X-rays, *Z. Kristallogr.*, in press.

31 S.B. Yi, C.H.J. Davies, H.-G. Brokmeier, R.E. Bolmaro, K.U. Kainer, J. Homeyer, Deformation and texture evolution in AZ31 magnesium alloy during uniaxial loading, *Acta Mater.* 2006, **54**, 549–562.

Edited by W. Reimers, A. R. Pyzalla,
A. Schreyer, H. Clemens

WILEY-VCH

Neutrons and Synchrotron Radiation in Engineering Materials Science

From Fundamentals to Material and Component Characterization